

Rare decays at the Tevatron

Daejung Kong^{*†}

Kyungpook Natinal University, Korea

E-mail: djkong@fnal.gov

Rare flavor changing neutral currents (FCNC) decays occur only through higher order diagrams in the Standard Model (SM) due to high suppression at tree level. FCNC processes have played an important role in connection to New Physics (NP). Decay rates and kinematic asymmetries provide excellent sensitivity to exchange of virtual NP particles. In this report we present recent measurements and current status on FCNC processes performed by the CDF and DØ Collaborations.

*The 13th International Conference on B-Physics at Hadron Machines - Beauty2011,
April 04-08, 2011
Amsterdam, The Netherlands*

^{*}Speaker.

[†]On behalf of the CDF and DØ Collaborations.

1. $b \rightarrow s\ell^+\ell^-$ transitions at CDF

The FCNC process $b \rightarrow s\ell\ell$ is prohibited at tree level, and occurs in the SM through higher order diagrams. Although the branching ratio of each $b \rightarrow s\ell\ell$ mode is quite small, $\mathcal{O}(10^{-6})$, the decay is experimentally clean due to opposite sign leptons. The exclusive channels $B^+ \rightarrow K^+\mu^+\mu^-$ and $B^0 \rightarrow K^{*0}\mu^+\mu^-$ have been observed at Belle [1, 2] and BaBar [3]. The analogous decay $B_s^0 \rightarrow \phi\mu^+\mu^-$ has not been observed. Typically B decays amplitudes are calculated using Wilson coefficients [4] through an Operator Product Expansion. The Wilson coefficients C_7 , C_9 , and C_{10} describe the perturbative part of the amplitudes from the electromagnetic penguin, the vector electroweak, and the axial-vector electroweak contributions, respectively. These amplitudes may interfere with non-SM contributions [5], therefore the transition can probe the presence of as yet unobserved particles and processes. More specifically, the lepton forward-backward asymmetry (A_{FB}) and the differential branching fraction as functions of dilepton invariant mass ($M_{\ell\ell}$) in the decays $B \rightarrow K^{*0}\ell^+\ell^-$ differ from the accurate SM expectations in various extended models [6]. Recently BaBar [7] and Belle [8] updated their A_{FB} measurements in the $B^0 \rightarrow K^{*0}\mu^+\mu^-$ mode. It is interesting that both experiments showed larger A_{FB} than the SM expectation including in the small q^2 region ($q^2 \equiv M_{\ell\ell}c^2$) where predictions are more accurate.

CDF has updated the analysis of $B^+ \rightarrow K^+\mu^+\mu^-$, $B^0 \rightarrow K^{*0}\mu^+\mu^-$ and $B_s^0 \rightarrow \phi\mu^+\mu^-$ with integrated luminosity of 4.4 fb^{-1} [9]. CDF obtains a signal yield for the $B^0 \rightarrow K^{*0}\mu^+\mu^-$ decay mode equal to 101 ± 12 (102 expected) and a signal yield for the $B^+ \rightarrow K^+\mu^+\mu^-$ equal to 121 ± 16 (142 expected). For the $B_s^0 \rightarrow \phi\mu^+\mu^-$ decay mode, we obtain 27 ± 6 (31 expected) decays, corresponding to a statistical significance of about 6σ . This is the first observation of the $B_s^0 \rightarrow \phi\mu^+\mu^-$ mode. Fig.1 shows the B mass distribution for each rare decay. The obtained branching ratios are consistent with world averages and theoretical expectations. The branching ratios are

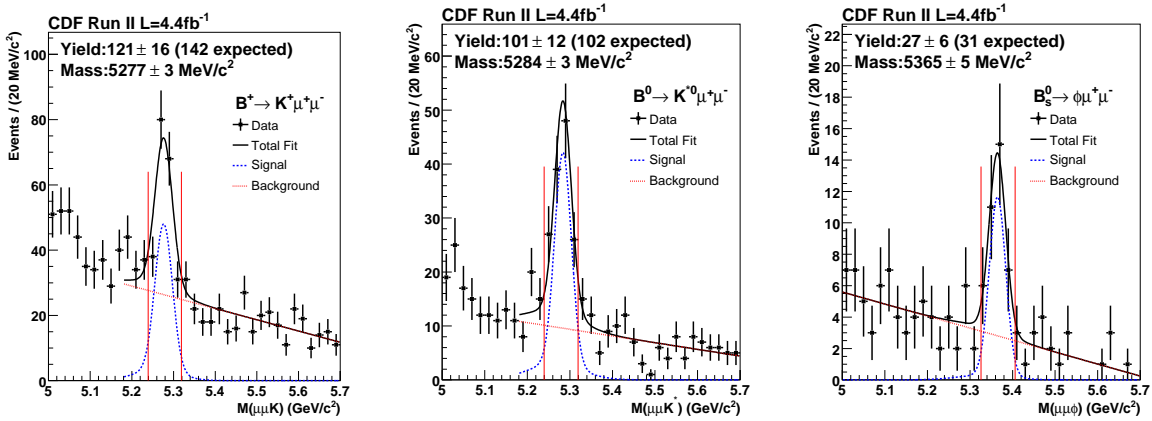


Figure 1: The B invariant mass of $B^+ \rightarrow K^+\mu^+\mu^-$, $B^0 \rightarrow K^{*0}\mu^+\mu^-$ and $B_s^0 \rightarrow \phi\mu^+\mu^-$ for 4.4 fb^{-1} at CDF, respectively. Histogram shows the data. Solid, dashed, and dotted curve shows total fit, signal PDF and background PDF, respectively. Fit range for $B^+ \rightarrow K^+\mu^+\mu^-$ and $B^0 \rightarrow K^{*0}\mu^+\mu^-$ ($B_s^0 \rightarrow \phi\mu^+\mu^-$) is from $5.18 \text{ GeV}/c^2$ ($5.00 \text{ GeV}/c^2$) to $5.70 \text{ GeV}/c^2$. Vertical lines show the signal region.

measured relative to the corresponding resonant control channels ($B \rightarrow J/\psi h$) using the relation:

$$\frac{\mathcal{B}(B \rightarrow h\mu^+\mu^-)}{\mathcal{B}(B \rightarrow J/\psi h)} = \frac{N_{h\mu^+\mu^-}^{NN}}{N_{J/\psi h}^{loose}} \cdot \frac{\epsilon_{J/\psi h}^{loose}}{\epsilon_{h\mu^+\mu^-}^{loose}} \cdot \frac{1}{\epsilon_{h\mu^+\mu^-}^{NN}} \cdot \mathcal{B}(J/\psi \rightarrow \mu^+\mu^-), \quad (1.1)$$

where $N_{h\mu^+\mu^-}^{NN}/(N_{J/\psi h}^{loose})$ are the $B \rightarrow h\mu^+\mu^-$ ($B \rightarrow J/\psi h$) yields after the optimal neural net cut (at the loose selection) requirement, $\epsilon_{J/\psi h}^{loose}/\epsilon_{h\mu^+\mu^-}^{loose}$ is the relative efficiency of the loose selection, $\epsilon_{h\mu^+\mu^-}^{NN}$ is the neural net (NN) cut efficiency of the loose selection sample. The NN selection is not applied to $J/\psi h$ channels, because the signals have sufficient purity even with the loose selection. The relative efficiencies and NN selection efficiencies are obtained from MC. The dimuon mass spectrum is cut off due to the charmonium veto in the mass ranges: $8.68 < M^2(\mu^+\mu^-) < 10.09(\text{GeV}/c^2)^2$ and $12.86 < M^2(\mu^+\mu^-) < 14.18(\text{GeV}/c^2)^2$, and both acceptance losses are corrected suitably. The absolute branching ratios are then obtained using world average values [10] for the control channel branching ratios:

$$\begin{aligned} \mathcal{B}(B^+ \rightarrow K^+\mu^+\mu^-) &= [0.38 \pm 0.05(\text{stat}) \pm 0.03(\text{syst})] \times 10^{-6}, \\ \mathcal{B}(B^0 \rightarrow K^0\mu^+\mu^-) &= [1.06 \pm 0.14(\text{stat}) \pm 0.09(\text{syst})] \times 10^{-6}, \\ \mathcal{B}(B_s^0 \rightarrow \phi\mu^+\mu^-) &= [1.44 \pm 0.33(\text{stat}) \pm 0.46(\text{syst})] \times 10^{-6}. \end{aligned}$$

This is the first measurement of the $B_s^0 \rightarrow \phi\mu^+\mu^-$ branching fraction, the rarest B_s^0 decay observed so far. These numbers are consistent with our previous results [11] and other B-factory measurements [7, 8, 12].

The forward-backward asymmetry (A_{FB}) and K^{*0} longitudinal polarization (F_L) in $B^0 \rightarrow K^{*0}\mu^+\mu^-$ decays are extracted from $\cos\theta_\mu$ and $\cos\theta_K$ distributions, respectively, where θ_μ is the helicity angle between the μ^+ (μ^-) direction and the opposite of the $B(\bar{B})$ direction in the dimuon rest frame, and θ_K is the angle between the kaon direction and the direction opposite to the B meson in the K^{*0} rest frame. CDF measures F_L and A_{FB} for $B^0 \rightarrow K^{*0}\mu^+\mu^-$ and also A_{FB} for $B^+ \rightarrow K^+\mu^+\mu^-$. Fit results are shown in Fig. 2. With the current experimental precision CDF data is unable to discriminate between the SM and non-SM scenarios, but the results are of comparable precision with B-factory results and could be combined with them for improved sensitivity.

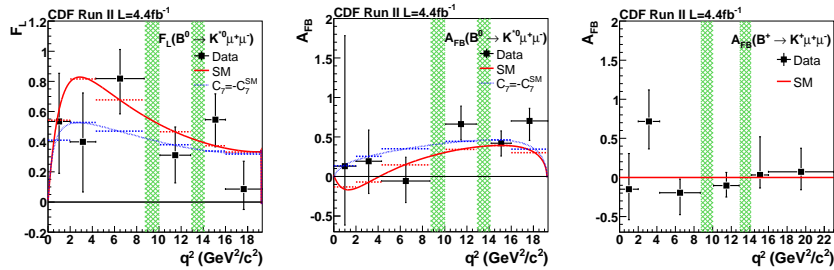


Figure 2: F_L and A_{FB} fit results for $B^0 \rightarrow K^{*0}\mu^+\mu^-$ and $B^+ \rightarrow K^+\mu^+\mu^-$ at CDF. From left to right, F_L and A_{FB} for $B^0 \rightarrow K^{*0}\mu^+\mu^-$ and A_{FB} for $B^+ \rightarrow K^+\mu^+\mu^-$ are shown. Histogram is the fit result, solid (dotted) curve is the SM ($C_7 = -C_7^{\text{eff}}$) expectation, dashed line is the averaged expectation in each q^2 bin, and hatched regions mean charmonium veto.

2. Search for rare $B_s^0(B^0) \rightarrow \mu^+\mu^-$ decay modes

The FCNC decays $B_s^0(B^0) \rightarrow \mu^+\mu^-$ occur in the SM only through higher order diagrams and are further suppressed by the helicity factor, $(m_\mu/m_B)^2$. The B^0 decay is also suppressed with respect to the B_s^0 decay by the ratio of CKM elements, $|V_{td}/V_{ts}|^2$. The SM expectations for these branching fractions are $\mathcal{B}(B_s^0 \rightarrow \mu^+\mu^-) = (3.2 \pm 0.2) \times 10^{-9}$ and $\mathcal{B}(B^0 \rightarrow \mu^+\mu^-) = (1.00 \pm 0.1) \times 10^{-10}$ [13], which are one order of magnitude smaller than current experimental sensitivity. New physics contributions can provide a significant enhancement to $B_s^0(B^0) \rightarrow \mu^+\mu^-$ [14, 15, 16, 17, 18]. CDF has performed an analysis of $B_s^0(B^0) \rightarrow \mu^+\mu^-$ with integrated luminosity of 3.7 fb^{-1} . CDF extract 95% (90%) C.L. limits of $\mathcal{B}(B_s^0 \rightarrow \mu^+\mu^-) < 4.3 \times 10^{-8}$ (3.6×10^{-8}) [19] and $\mathcal{B}(B^0 \rightarrow \mu^+\mu^-) < 7.6 \times 10^{-9}$ (6.0×10^{-9}) [19], which are currently the world best upper limits for both processes. DØ performs a similar analysis. Latest results are based on a data sample of integrated luminosity of 6.1 fb^{-1} . The observed event rates are, also in this case, consistent with SM background expectations. DØ extract 95(90)% C.L. limits of $\mathcal{B}(B_s^0 \rightarrow \mu^+\mu^-) < 5.1 \times 10^{-8}$ (4.2×10^{-8}) [20]. The distribution of DØ's signal enhancing Neural Net output (see [20] for details) and observed distributions of dimuon events in the highest sensitivity region are shown in Fig. 3. CDF is currently updating the analysis on a data sample of 7 fb^{-1} of integrated luminosity. The sensitivity of this analysis is significantly improved by increasing the event sample size, increasing the trigger acceptance, and by using an enhanced muon selection and an improved neural network (NN) discriminant which provides approximately 25% better background rejection for the same signal efficiency compared to the previous published analysis [21].

The CDF II detector is described in detail in Ref. [22]. Charged particle tracking is provided by a silicon microstrip detector surrounded by an open-cell wire drift chamber immersed in a 1.4 T solenoidal magnetic field. This system provides precise vertex determination and momentum measurements for charged particles in a pseudorapidity range $|\eta| < 1.0$, where $\eta = -\ln(\tan \frac{\theta}{2})$ and

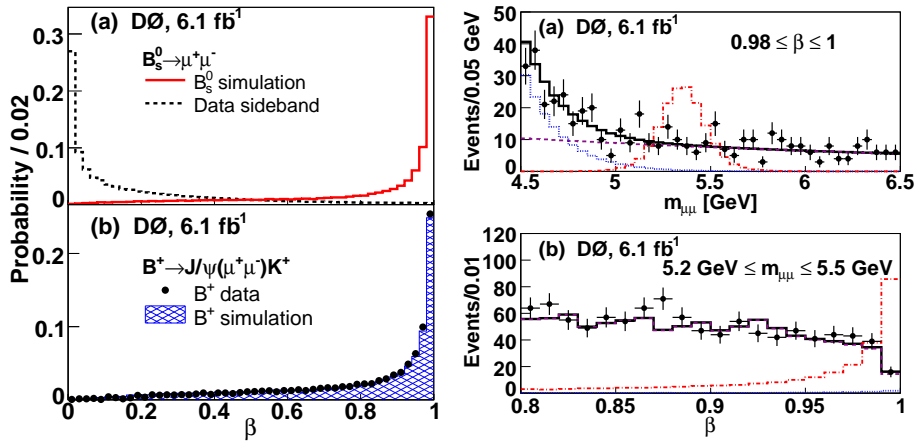


Figure 3: NN output and Mass distribution with integrated luminosity 6.1 fb^{-1} at DØ. Left: Distributions of: (a) $B_s^0 \rightarrow \mu^+\mu^-$ signal and sideband events, (b) $B^+ \rightarrow J/\psi(\mu^+\mu^-)K^+$ data and simulation. Right: The distribution of $m_{\mu\mu}$ in the highest sensitivity β region (a), and the distribution of β in the highest sensitivity $m_{\mu\mu}$ region (b) for data (dots with uncertainties), expected background distribution (solid line), and the SM signal distribution multiplied by a factor of 100 (dotted dashed line).

θ is the angle of the track measured with respect to the proton beam direction. Additionally, the drift chamber measures the ionization per unit path length, dE/dx , for particle identification. Surrounding the tracking detectors are electromagnetic and hadronic sampling calorimeters arranged in a projective geometry. Drift chambers are located behind the calorimeters to detect muons in the central region (C) $|\eta| < 0.6$ and the forward region (F) $0.6 < |\eta| < 1.0$.

The offline reconstruction begins by identifying two muon candidates of opposite charge which satisfy the online dimuon trigger requirements. Events must have satisfied either of two sets of requirements implemented in the online trigger system as described in detail in Refs. [22, 23]. The data used in this analysis are selected by two classes of dimuon triggers: for the CC triggers, both muon candidates are reconstructed in the central region, while for the CF triggers, one of the muon candidates is reconstructed in the forward region. The acceptance of the analysis is improved by 20% by using additional forward muon candidates and by using muon candidates that traverse detector regions previously excluded due to their rapidly changing trigger efficiency. Since they have different sensitivities, we treat CC and CF channels separately, combining the results at the end. Two oppositely charged muon candidates are selected within a dimuon invariant mass window of $4.669 < m_{\mu\mu} < 5.969 \text{ GeV}/c^2$ around the B_s^0 and B^0 masses. Backgrounds from hadrons misidentified as muons are suppressed by selecting muon candidates using a likelihood function. This function tests the consistency of electromagnetic and hadronic energy with that expected for a minimum ionizing particle and the differences between extrapolated track trajectories and muon system hits [24]. In addition, backgrounds from kaons that penetrate through the calorimeter to the muon system or decay in flight outside the drift chamber are further suppressed by a loose selection based on the measurement of the ionization per unit path length, dE/dx [25]. The inputs to the muon likelihood and the dE/dx performance are calibrated using samples of $J/\psi \rightarrow \mu^+\mu^-$ and $D^0 \rightarrow K^-\pi^+$ decays. To reduce combinatorial backgrounds the muon candidates are required to have transverse momentum relative to the beam direction $p_T > 2.0 \text{ GeV}/c$, and $|\vec{p}_T^{\mu\mu}| > 4 \text{ GeV}/c$, where $\vec{p}_T^{\mu\mu}$ is the transverse component of the sum of the muon momentum vectors. The remaining pairs of muon tracks are fit under the constraint that they come from the same three-dimensional (3D) space point. To achieve further separation of signal from background, we employ additional discriminating variables. These include the measured proper decay time, λ ; the proper decay time divided by the estimated uncertainty, λ/σ_λ ; the 3D opening angle between vectors $\vec{p}_T^{\mu\mu}$ and the displacement vector between the primary vertex and the dimuon vertex, $\Delta\Theta$; and the B-candidate track isolation, I . We require $\lambda/\sigma_\lambda > 2$, $\Delta\Theta < 0.7 \text{ rad}$, and $I > 0.50$. The baseline selection reduces combinatorial backgrounds by a factor of 300 while keeping approximately 50% of the signal events that are within the acceptance (geometric and kinematic requirements) of the trigger. A sample of $B^+ \rightarrow J/\psi K^+$ events is collected to serve as a normalization mode using the same baseline requirements, but including a requirement of $p_T > 1 \text{ GeV}/c$ for the kaon candidate and constructing the $B^+ \rightarrow J/\psi K^+ \rightarrow \mu^+\mu^-$ vertex using only the muon candidate tracks.

Information from the following 14 variables is used to construct a NN discriminant (v_N) that enhances signal to background discrimination [26]: λ/σ_λ , λ , $\Delta\Theta$ and I are defined above; L , the magnitude of the displacement vector between the primary vertex and the dimuon vertex; L_T/σ_{L_T} , the significance of the displacement vertex evaluated in the plane transverse to the beamline; $\Delta\Theta_T$, a two dimensional projection of $\Delta\Theta$ in the plane transverse to the beamline; χ_{vtx}^2 , the χ^2 of the secondary vertex fit; $|d_0^{\text{max}}|$ and $|d_0^{\text{min}}|$, the unsigned impact parameters, of each muon in descending

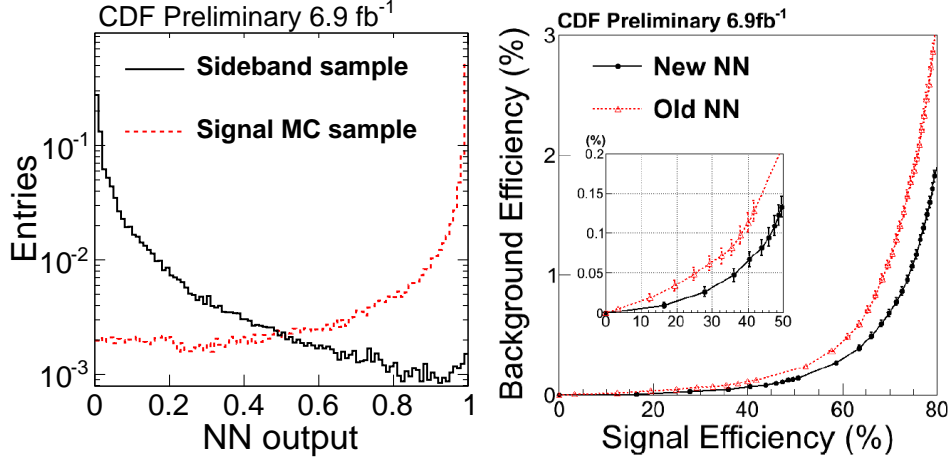


Figure 4: Left : The distribution of NN output at CDF, the red histogram is the signal MC and the black histogram is sideband data. Right : Background efficiency as function of signal efficiency, black is new NN and red is old NN.

order, where impact parameter is defined as the distance of closest approach of the track's trajectory to the primary vertex in transverse plane; $|d_0^{\max}|/\sigma_{d_0}^{\max}$ and $|d_0^{\min}|/\sigma_{d_0}^{\min}$, the significance of the muon impact parameters; $d_0(B_s^0)$, the impact parameter of the B_s^0 candidate; the lower of the muon transverse momenta. The NN is trained with background events sampled from the sideband regions and signal events generated with a simulation described below. One-third of the background sample is used for NN training, the remaining two-thirds is reserved to test the background discrimination. Statistically independent signal samples are used for training and testing the efficiency of the NN. Several tests are done to ensure the v_N is uncorrelated with $m_{\mu\mu}$ to avoid sculpting the background mass distribution. The NN achieves strong discrimination against background as shown in Fig.4. The expected background is obtained by summing contributions from the combinatorial continuum and from $B \rightarrow h^+h^-$ decays, which peak in the B_s^0 and B^0 invariant mass signal region and do not occur in the sidebands. The contribution from other heavy-flavor decays is negligible. The combinatorial background is estimated by linearly extrapolating from the sideband region to the signal region.

A relative normalization is used to determine the $B_s^0 \rightarrow \mu^+\mu^-$ branching fraction:

$$\mathcal{B}(B_s^0 \rightarrow \mu^+\mu^-) = \frac{N_s}{N_+} \cdot \frac{\alpha_+}{\alpha_s} \cdot \frac{\epsilon_+}{\epsilon_s} \cdot \frac{1}{\epsilon_N} \cdot \frac{f_u}{f_s} \cdot \mathcal{B}(B^+ \rightarrow J/\psi K^+), \quad (2.1)$$

where N_s is the number of $B_s^0 \rightarrow \mu^+\mu^-$ candidate events. The observed number of $B^+ \rightarrow J/\psi K^+$ candidates is $N_+ = 21,471 \pm 191$ and $9,814 \pm 137$ in CC and CF channels, respectively. The contribution of $B^+ \rightarrow J/\psi \pi^+$ events is negligible. The parameter α_+ (α_s) is the acceptance of the trigger and ϵ_+ (ϵ_s) is the efficiency of the reconstruction requirements for the signal (normalization) mode. The ratios of acceptances α_+/α_s are 0.300 ± 0.018 and 0.196 ± 0.014 for the CC and CF topologies, respectively. These ratios are measured using simulated events, and its uncertainty includes contributions from systematic variations of the modeling of the B-hadron p_T distributions, the longitudinal beam profile, and from the statistics of the simulated event samples. The reconstruction

efficiency includes trigger, track, muon, and baseline selection efficiencies. The ratio of reconstruction efficiencies is $\varepsilon_+/\varepsilon_s = 0.81 \pm 0.03$ as determined from studies using samples of $J/\psi \rightarrow \mu^+\mu^-$ and $B^+ \rightarrow J/\psi K^+$ events collected with the same triggers. The uncertainty in $\varepsilon_+/\varepsilon_s$ is dominated by kinematic differences between $J/\psi \rightarrow \mu^+\mu^-$ and $B_s^0(B^0) \rightarrow \mu^+\mu^-$ decays. The NN efficiency, ε_N , is estimated from the simulation. We use $\mathcal{B}(B^+ \rightarrow J/\psi K^+) = (6.01 \pm 0.21) \times 10^{-5}$ and the ratio of B-hadron production fractions $f_u/f_s = 3.55 \pm 0.47$ [10]. The expression for $\mathcal{B}(B^0 \rightarrow \mu^+\mu^-)$ is derived by replacing B_s^0 with B^0 and the fragmentation ratio with $f_u/f_d = 1$. Muon reconstruction efficiencies are estimated as a function of muon p_T using observed event samples of inclusive $J/\psi \rightarrow \mu^+\mu^-$ decays.

The expected background is obtained by summing contributions from the combinatorial continuum and from $B \rightarrow h^+h^-$ decays. We estimate the combinatorial background by linearly extrapolating from the sideband region to the signal region. We fit the $m_{\mu\mu}$ distribution of sideband events with $v_N > 0.70$ to a linear function. We only use events with $m_{\mu\mu} > 5 \text{ GeV}/c^2$ in order to suppress contributions from $b \rightarrow \mu^+\mu^-X$ decays. The slopes are then fixed, and the normalization is determined for each v_N bin separately using the relevant sideband events. The $B \rightarrow h^+h^-$ contributions are estimated using efficiencies taken from the simulation, probabilities of misidentifying hadrons as muons measured in a $D^0 \rightarrow K^-\pi^+$ data sample, and normalizations derived from branching fractions from Refs. [15, 17]. The two-body invariant mass distribution of the simulated $B \rightarrow h^+h^-$ candidates is calculated from the momentum of the hadrons assuming the muon mass hypothesis. The background estimates are cross-checked using three independent control samples: $\mu^\pm\mu^\pm$ events, $\mu^+\mu^-$ events with $\lambda < 0$, and a misidentified muon-enhanced $\mu^+\mu^-$ sample in which we require one muon candidate to fail the muon quality requirements. We compare the predicted and observed number of events in these samples for a wide range of v_N requirements and observe no significant discrepancies. The signal region is divided into five equal mass bins of $24 \text{ MeV}/c^2$ and eight v_N bins delineated at 0.7, 0.76, 0.85, 0.90, 0.94, 0.97, 0.987, 0.995 and 1.0. The backgrounds, efficiencies, and limits are calculated in each bin separately. Using a data sample of 7 fb^{-1} of integrated luminosity, collected by CDF experiment, we calculate approximate expected 95% C.L. limits of 2×10^{-8} for $B_s^0 \rightarrow \mu^+\mu^-$. The limit is estimated from Eq. 2.1 using the confidence level (CLs) method of Ref. [27] to extract the 95% C.L. upper bound on N_s ; the limit incorporates Gaussian uncertainties on the signal acceptance and efficiency as well as the background estimates.

3. Summary and outlook

FCNC decays provide powerful probes of new physics. The CDF and DØ experiments currently provide the most stringent limits on these decays. CDF reports the first observation of $B_s^0 \rightarrow \phi\mu^+\mu^-$ using 4.4 fb^{-1} of integrated luminosity, the most rare B_s^0 decay observed to date, and measures its total branching ratio. CDF measures the total branching ratio, differential branching ratio, and forward-backward asymmetry of the processes $B^+ \rightarrow K^+\mu^+\mu^-$ and $B^0 \rightarrow K^{*0}\mu^+\mu^-$, with respect to q^2 . CDF also measures the K^{*0} longitudinal polarization in $B^0 \rightarrow K^{*0}\mu^+\mu^-$. These are consistent and competitive with the best published results. At present there is no evidence of discrepancy from SM predictions. CDF has currently the most stringent limits on the decay rate of

$B_s^0 \rightarrow \mu^+ \mu^-$ which significantly constrain large regions of NP parameters space. Improved results are expected when the analysis will be extended to the full run II data sample.

References

- [1] K. Abe *et al.* (BELLE Collaboration), *Phys. Rev. Lett.* **88**, 021801 (2002).
- [2] A. Ishikawa *et al.* (BELLE Collaboration), *Phys. Rev. Lett.* **91**, 261601 (2003).
- [3] B. Aubert *et al.* (BABAR Collaboration), *Phys. Rev. Lett.* **91**, 221802 (2003).
- [4] K. G. Wilson, *Phys. Rev.* **179**, 1499 (1969).
- [5] G. Burdman, *Phys. Rev. D* **52**, 6400 (1995).
- [6] W. S. Hou *et al.*, *Phys. Rev. D* **77**, 104016 (2008).
- [7] B. Aubert *et al.* (BABAR Collaboration), *Phys. Rev. D* **79**, 031102 (2009).
- [8] J. T. Wei *et al.* (BELLE Collaboration), *Phys. Rev. Lett.* **103**, 171801 (2009).
- [9] T. Aaltonen *et al.* (CDF Collaboration), *Phys. Rev. Lett.* **106**, 161801 (2011).
- [10] K. Nakamura *et al.* (Particle Data Group), *J. Phys. G* **37**, 075021 (2010).
- [11] T. Aaltonen *et al.* (CDF Collaboration), *Phys. Rev. D* **79**, 011104 (2009).
- [12] B. Aubert *et al.* (BABAR Collaboration), *Phys. Rev. Lett.* **102**, 091803 (2009).
- [13] A. J. Buras *et al.*, *JHEP* **106**, 1009 (2010).
- [14] S. R. Choudhury and N. Gaur, *Phys. Lett. B* **451**, 86 (1999); K.S. Babu and C. Kolda, *Phys. Rev. Lett.* **84**, 228 (2000).
- [15] R. Arnowitt *et al.*, *Phys. Lett. B* **538**, 121 (2002).
- [16] S. Baek *et al.*, *JHEP* **0506**, 017 (2005).
- [17] R. Ruiz de Austri *et al.*, *JHEP* **0605**, 002 (2006); J. Ellis *et al.*, *J. High Energy Phys.* 0605, 063 (2006).
- [18] P. H. Chankowski and J. Rosiek, *Acta Phys. Pol. B* **33**, 2329 (2002).
- [19] CDF Collaboration, Public Note 9892.
- [20] V. M. Abazov *et al.*, (D0 Collaboration), *Phys. Lett. B* **693**, 539 (2010).
- [21] D. Aaltonen *et al.* (CDF Collaboration), *Phys. Rev. Lett.* **100**, 101802 (2008).
- [22] D. Acosta *et al.* (CDF Collaboration), *Phys. Rev. D* **71**, 032001 (2005).
- [23] D. Acosta *et al.* (CDF Collaboration), *Phys. Rev. Lett.* **93**, 032001 (2004).
- [24] D. Abulencia *et al.* (CDF Collaboration), *Phys. Rev. Lett.* **97**, 242003 (2006).
- [25] D. Abulencia *et al.* (CDF Collaboration), *Phys. Rev. Lett.* **97**, 211802 (2006).
- [26] M. Feindt and U. Kerzel, *Nucl. Instr. Meth. A* **559**, 190 (2006).
- [27] W.-M. Yao *et al.*, *J. Phys. G* **33**, 1 (2006).